Creep and oxidation kinetics at 1100°C of nickel-base alloys reinforced by hafnium carbides

Patrice Berthod, Elodie Conrath

Creep and oxidation kinetics at 1100°C of nickel-base alloys reinforced by hafnium carbides

Patrice Berthod*, Elodie Conrath

Institut Jean Lamour (UMR CNRS 7198),
Team 206 « Surface and Interface : Chemical Reactivity of Materials »,
Faculty of Science and Technologies, University of Lorraine,
Postal Box 70239, F-54506 Vandoeuvre-lès-Nancy, France

* *Corresponding author: pberthodcentralelille1987@orange.fr*

Postprint of the article *Materials and Design 104 (2016) 27–36*
http://dx.doi.org/10.1016/j.matdes.2016.04.079

Keywords: Ni-Cr-C-Hf alloys, high temperature, flexural creep, oxidation kinetic

Abstract

The mechanical reinforcement of polycrystalline alloys at elevated temperature may be achieved by HfC carbides. Generally such alloys must be also resistant against oxidation by hot gases and corrosion by molten substances. Polycrystalline chromium-rich nickel-based alloys represent a good solution for answering these requirements about the high temperature chemical resistance. Unfortunately they tend to be rather mechanically weak at high temperature compared to γ/γ' single crystals. In this work a new family of alloys, combining a chromium-rich nickel-based matrix and an interdendritic HfC carbide network, is studied. Two equiaxed cast alloys were elaborated by classical foundry and the obtained microstructures were examined. Two types of high temperature properties were characterized at 1100°C, creep resistance and oxidation kinetic.

The microstructures of the two alloys are composed of a dendritic austenitic matrix and of script-like eutectic carbides which are recognized to be very favorable for high strength at high temperature. Creep tests proved this potential benefit by showing that these alloys are much more resistant than usual cast polycrystalline nickel-based alloys. The base made of nickel and the 25 wt.% content in chromium allow obtaining a chromia-forming behavior leading to good resistance against oxidation in hot air.

1. Introduction

The γ'-reinforced Ni-based single-crystal alloys are surely still the best superalloys for applications at elevated temperatures [1]. Exceptional mechanical properties are brought by their dense population of Ni_3Al ideally-sized particles precipitated with crystallographic coherency with the matrix. This efficient precipitation hardening can be obtained by multistep heat treatment carried out in ideal conditions thanks to the total absence of grain boundaries. These single-crystals can be solution treated at very high temperature to totally dissolve the undesirable compounds formed during solidification, and then to optimize the results of the precipitation treatment [2-8]. These single-crystals alloys also exhibit excellent resistance against oxidation by hot gases and corrosion by molten sulfates thanks to the simultaneous presence of aluminum and (of rather small) quantity of chromium [9].

However such single-crystal alloys are essentially devoted to constitute slender pieces such as turbine blades and they cannot be solidified with more complex shapes. In the later cases powder metallurgy (PM) or conventional casting must be considered. When high mechanical resistance is required at temperatures higher than 1000°C, the small grains of alloys issued from PM process [10-15] are not suitable, unlike the coarser grains resulting from casting [16-21].

Although used rather for disk [22] than for blades, polycrystalline nickel-based alloys elaborated by casting may be considered for high temperature under stress [23, 24]. They can contain high quantities of chromium (instead aluminum) to resist both oxidation by gases and corrosion by many types of molten substances. The latter one is not efficient in all situations of high temperature corrosion (e.g. contact with molten glasses [25, 26]) and its presence is not as necessary as for γ-γ' single-crystals.

Besides precipitation hardening and solid solution strengthening, cast polycrystalline nickel-based alloys may be reinforced by primary carbides resulting from final eutectic solidification. The carbides which are often present in cast superalloys are chromium carbides of the M_7C_3 or $M_{23}C_6$ types [27-30], to which other elements may also belong (tungsten, molybdenum…). These carbides are not stable at high temperature and they tend to partially, and sometimes totally, dissolve at temperatures as high as 1100°C. This phenomenon is also encountered in cobalt-based superalloys in which MC carbides, notably tantalum carbides (TaC) [31-34], are more stable. Furthermore, these TaC carbides obtained in cobalt-based superalloys present a script-like morphology issued from their eutectic solidification with matrix. This shape leads to an efficient interdendritic cohesion and thus to high mechanical

resistance at high temperature. Obtaining TaC carbides in Ni-based alloys was attempted in a recent study [35], but this was not successful since the TaC carbides were, on the contrary, less stable than chromium carbides in the microstructure of such alloys. Other elements such as titanium an niobium also may lead to the formation of MC carbides in nickel-based superalloys [36], but the obtained particles tend to degenerate during long-term exposures at high temperature [37, 38] and basing the mechanical strengthening of Ni-based superalloys must involve other MC-former elements.

The reinforcement of cast polycrystalline alloys using another type of MC carbides was recently considered by choosing hafnium instead tantalum. This element, which is much more known for its beneficial effect for high temperature oxidation [39-42], notably in thermal cycling, was added to chromium-rich nickel-based alloys in which it strongly favors the precipitation of primary HfC carbides instead chromium carbides [43]. Exposures at 1200°C applied to the obtained alloys [44] demonstrated that these carbides were much more stable at high temperature than chromium carbides in nickel alloys, and even more than the TaC carbides present in some cobalt-based superalloys. The oxidation behavior at 1200°C of the obtained alloys was rather good [45] but, unfortunately, their creep resistance was catastrophic at this temperature [46]. These previous studies showed that HfC-reinforced nickel-based alloys may be used at 1200°C but in absence of applied stress.

Thinking that the poor mechanical resistance at 1200°C is may be due more to the weak nickel base of the alloys than to a lack of reinforcement by the HfC carbides, it was decided to mechanically characterize one of the alloys at a lower temperature, 1100°C. This one is still a service temperature for which γ-γ' single-crystalline nickel-based superalloys are not yet suitable because of a significant dissolution of their reinforcing intermetallic precipitates.

In this work, two chromium nickel-based superalloys reinforced partly or exclusively by HfC carbides, elaborated by conventional casting were considered for the study of their properties at 1100°C. They were subjected to 3-points flexural creep test under 20 MPa and their behavior in oxidation was verified at 1100°C by thermogravimetry tests and post-mortem characterization of the oxidized samples.

2. Materials design

The two alloys considered in this work were elaborated by targeting the following compositions: Ni(bal.)-25Cr-0.50C-3.7Hf and Ni(bal.)-25Cr-0.50C-5.6Hf (all contents in weight percent). Their were elaborated by foundry from pure elements (all from Alfa Aesar, purity > 99.9 wt.%). Fusion and solidification were achieved in the water-cooled copper

crucible of a High Frequency Induction furnace (CELES), under an inert atmosphere of pure Ar (about 300 mbars). The two solidified ingots (weighing about 40g) were cut after total cooling and exit from the furnace. This was done first by using a Buelher Delta Abrasimet cutter for obtaining two halves of each compact ingot. In a second step, for better accuracy, this was a Buelher IsoMet 5000 precision saw which was used.

A Hf-free ternary alloy with the same contents in Cr and C was added to the study in order to specify the effect of the presence of hafnium on the oxidation behavior of the two Hf-containing alloys. This additional alloy was elaborated and machined in the same conditions as for the two first ones. The names and the targeted chemical compositions of the two Hf-containing alloys (NiHf2-1 and NiHf2-2) and of the ternary alloy added for comparison (NiHf2), are given in Table 1.

3. Experimental procedure

Three types of samples were prepared: compact ones for the metallographic characterization of the microstructures of the as-cast alloys, elongated parallelepipeds for performing creep bending tests, and square-based parallelepipeds for the oxidation tests in thermo-balance.

The first ones were embedded in a cold resin mixture (ESCIL: CY230 resin and HY956 hardener), then ground with 250 to 1200-grit SiC papers. After ultrasonic cleaning in water, they were polished with textile enriched with 1µm-sized hard particles for obtaining a mirror-like state. The second ones, whose dimensions were 1mm (thickness) × 2mm (width) × 15mm (length), were accurately cut, before being polished with papers up to 1200-grit with final strips in the length direction. These parallelepipeds, homogeneous thickness and width (tolerance: ±0.01 mm, controlled using an electronic caliper), were visually inspected, and thereafter thoroughly examined by microscopy (optical and/or electronic) to be sure that no defects able to weaken the samples were present. The third samples were prepared to perform high temperature oxidation tests, with dimensions of about 8mm × 8mm × 3mm. They were polished all around with 1200-grit SiC papers with smoothing of their edges and corners.

After embedding and polishing the metallographic samples were observed using a Scanning Electron Microscope (SEM, type: JEOL JSM6010LA). Observations were done under an accelerating voltage of 20kV and in the Back Scattered Electrons (BSE) mode. The different applied magnifications were ×125, 250, 500 and 1000. The obtained chemical compositions were measured on the as-cast samples using the Energy Dispersive Spectrometry (EDS) device attached to the SEM. The different phases were specified by EDS spot analyses.

The surface fractions of the different types of carbides present in the as-cast microstructures of the alloys were measured on SEM/BSE micrographs by using the image analysis tool of the Photoshop CS software of Adobe.
Indentations were carried out for the three alloys at room temperature using a Testwell apparatus, to measure their Vickers hardness. In each case ten indentations were performed under a 10kg load; an average value and a standard deviation one were calculated.

The two Hf-containing alloys were submitted to bending tests at 1100°C under constant load, according to the symmetrical three point flexural method. A high temperature dilatometer (SETARAM, TMA92-16.18) modified to allow 3-points flexural testing (alumina equipment supplied by SETARAM) was used in each case. Both tests were done under pure argon. The space between the two bottom supports was 12 mm and the maximal possible deformation was about 1.4 mm (height of these supports). The load was applied to the sample by the upper support. This induced a 20MPa tensile stress in the middle of the bottom side of the sample. Its value was accurately calculated for each sample by taking into account the exact values of their thickness and width. The principle of this test as well as the relationship between the geometrical dimensions, the wished maximal tensile stress and the load to apply, are reminded together in Figure 3. The load was progressively applied at room temperature, until reaching the targeted value. Sample and supports were then heated at a constant rate of 20°C min^{-1}, before the isothermal stage. This one was more or less long, depending on the behavior of the tested sample. The downward vertical displacement of the upper support was recorded every 36 seconds during the whole experiment. At the end of the experiment a cooling was applied at a rate of -20°C min^{-1}.

The three alloys were tested in oxidation at high temperature using a SETARAM TG-92 thermo-balance. Each sample was exposed to synthetic dry air 80%N_2-20%O_2 during 46 hours at 1100°C after a heating at 20°C min^{-1}. At the end of the isothermal stage the external cooling was realized at -5°C min^{-1}. X-ray diffraction (XRD) runs were carried out to characterize the oxides scales. The oxidized samples were thereafter covered by a thin gold coating, then by a thick nickel coating (2 hours of an electrolytic deposition in a 50°C-heated Watt's bath under a 0.02A cm^{-2} density of current This was realized in order to mechanically protect the oxide scales during cutting. The coated oxidized samples were cut, embedded with cold resin and polished until obtaining a mirror-like state. They were examined using the

SEM in BSE mode. The sub-surfaces and the oxide scales were subjected to spot EDS analysis (identification and concentration profiles in the Cr-depleted zone).

4. Results and Discussion

4.1. Microstructure and hardness prior to the high temperature tests

The as-cast microstructures of the two Hf-containing alloys are illustrated in Figure 1 and Figure 2 by SEM/BSE micrographs taken at two magnifications: ×250 for general view and ×1000 for more details about the geometry of the carbides. They can be compared to the ones of the NiHf2 (reference alloy, classical dendritic matrix with interdendritic chromium carbides) presented in Figure 3. The two alloys are composed of a dendritic matrix and of interdendritic carbides (surface fractions presented in Table 2, together with the result for the reference NiHf2 alloy). In the NiHf2-1 alloy, whose composition is Ni(bal.)-25Cr-0.50C-3.7Hf, in wt.%), the carbides are mainly hafnium carbides but some chromium carbides are also present. In contrast only HfC carbides are present in the NiHf2-2 alloy (Ni-25Cr-0.50C-5.6Hf, in wt.%). Their fraction is equal to twice the ones of the previous alloy.
Vickers indentations carried out with a load of 10kg on the alloys led to 224±9 for NiHf2-1 and 243±4 for NiHf2-2 (both harder than NiHf2: 216±9).

4.2. Creep behavior

When subjected to three points bending test at 1100°C under constant load (principle reminded in Figure 4), these alloys show a rather good resistance against creep deformation. Indeed, for a central load inducing a tensile stress of 20MPa in the middle of the bottom side of the parallelepiped samples, the deformations of the NiHf2-1 and NiHf2-2 alloys are very slow (about 0.6 and 1.6 $\mu m\ h^{-1}$ respectively, in the secondary creep stage). The deformation curves of the NiHf2-1 and NiHf2-2 alloys are presented in Figure 5 and Figure 6 respectively. Figure 7 shows the NiHf2-2 sample after a 200 hours creep test, by a macrograph showing its global creep deformation and a micrograph illustrating the microstructure and the surface damaged state where the 20MPa stress were applied (no cracks).

4.3 Oxidation behavior - kinetic analysis

The thermogravimetry curves obtained for the two Hf-containing alloys at 1100°C during 46 hours in dry synthetic air are plotted in the graph presented in Figure 8, with the one obtained

for the Hf-free one for comparison (mass gain per surface unit area, noted m (g/cm^2), versus time). As frequently observed for chromium-rich nickel-based alloys the kinetic is parabolic for each of the three studied alloys, without any jumps in mass gain due to oxide detachment from substrate. They are quite regular and the mass gains achieved after 46 hours are typical of a chromia-forming behavior. This is the reason why the three files were analyzed according to the {m×dm/dt = Kp - Kv × m} method [47] which allows the simultaneous determination of the parabolic constant Kp and of the volatilization constant Kv, with as important consequence no underestimation of the parabolic constant. An example of such numerical treatment is given in Figure 9. Additionally, since the mass gain is often linear at the early beginning of the isothermal stage, a value of the linear constant Kl is determined by calculating the slope of the short initial linear mass gain.

The obtained values for the three constants are given in Table 3. The linear constant Kl has the same value for the NiHf2 and NiHf2-2 alloys (about 20×10^{-8} g cm^{-2} s^{-1}) while the NiHf2-1 alloy led to half this value. When classically determined (by plotting the mass gain versus the square root of time), the NiHf2-1 alloy seems to oxidize very slowly (Kp only of about 1×10^{-12} g^2 cm^{-4} s^{-1}), by considering the rather high temperature of the test. The Hf-free NiHf2 alloy presents a Kp value equal to four times the NiHf2-1. The fastest oxidation was the one of the NiHf2-2 alloy, with a Kp value equal to twice the NiHf2 one.

Plotting the m×dm/dt quantity versus –m allows determining the Kp constant (ordinate at the origin) and the Kv one (slope of the straight line). Concerning the parabolic constant, the order remains globally the same between the three alloys, but all the Kp values are greater than the previous values classically determined before. Indeed, at 1100°C, chromia volatilization takes place and the determination of the real Kp constants necessitates to take the linear mass loss rate into account. Obviously, the chromia volatilization rate Kv depends on the Hf content: the lowest value is the one of the Hf-free ternary alloy, and the highest one is the one of the NiHf2-2 one. These values were all validated by plotting mathematical curves using these Kp and Kv values and by comparing the obtained curves to the experimental ones (Figure 10). Comparisons showed that the determined {Kp, Kv} couples of values led to model curves (“KpcorrKv”) which well fitted the experimental mass gain curves (“exp mass gain”) much more the model curves plotted with the classically determined Kp values (“classic Kp”).

4.4 Oxidation behavior - post mortem characterization

The oxidized samples have more or less lost their external oxide scales, as illustrated by photographs presented in Figure 11 (obtained with a simple office scanner). The Hf-containing NiHfC2-1 and NiHfC2-2 alloys have kept almost their scales while oxide spallation occurred during the cooling of the Hf-free NiHf2 alloy. XRD runs (Figure 12) were thus performed to specify the natures of the oxides present in these scales and it appears that chromia was in all cases the main oxide present on the surfaces of the three oxidized samples. However the presence of nickel oxide and of the spinel oxide $NiCr_2O_4$ was detected in all cases while the HfO_2 oxide was present in the scales of the two oxidized Hf-containing alloys. Cross-sections were prepared for SEM/BSE observations (Figure 13). The examinations confirm the results of the XRD runs. They also allow seeing that the subsurface of the Hf-containing alloys are only a little damaged by oxidation. If the chromium carbides have disappeared over a more or less deep part of the alloy from the oxide/alloy interface (NiHf2 and NiHf2-1 alloys) the population of HfC carbides is not changed in the NiHf2-1 and NiHf2-2 alloys, neither in the subsurface, nor in the bulk. The Cr contents remained still high in the alloy very close to the interface, as shown by spot EDS analyses whose results are given in Table 3. They are especially high for the two Hf-containing alloys (more than 22 wt.%). In contrast, Hf is almost absent in the matrix.

4.5. Discussion

The two nickel-based alloys of this study were wished with a dendritic austenitic matrix and an interdendritic network of carbides mainly constituted of eutectic script-like HfC. This was obviously successful since many HfC carbides effectively appeared during solidification, and furthermore they remained stable during a long stage at 1100°C. Neither their volume fraction nor their morphology evolved significantly in the bulk of the samples during the 46 hours spent at 1100°C, and even during the 200 hours spent at this same high temperature for the creep-test samples. Thus, in contrast with tantalum carbides (TaC) which are less stable than chromium carbides in Cr-rich nickel-based [32] alloys, Hf leads to carbides as stable in such alloys as in Cr-rich cobalt-based [41] and iron-based alloys [42].

Usually, the existence of a carbide network in metallic alloy whose matrix hardness is rather low (as here for nickel-based ones), may induce an increase in hardness for the whole alloy, as soon as this carbide network is at least a little continuous. This is the case here for the three alloys (chromium carbides and/or HfC network). In addition the increase amplitude in alloy hardness tends to be higher for a higher hardness of the carbides. Here, the presence of these

primary interdendritic HfC carbides first led to increase in hardness by comparison with the two alloys which contain chromium carbides. This can be due to the higher intrinsic hardness of the HfC carbides (2913Hv_{50g} [43]) by comparison the chromium carbides in general (1650 Hv_{50g} for $Cr_{23}C_6$, 1336 Hv_{50g} for Cr_7C_3 or 1350 Hv_{50g} for Cr_3C_2 [43]), but also to the special morphology and the greater volume fraction which were obtained with hafnium carbides, in the NiHf2-1 and NiHf2-2 alloys, than with the chromium carbides in the NiHf2 one.

Although hardened by the HfC carbides the alloys are still easy to machine at ambient temperature. These hardness values let expecting interesting creep resistance. This is effectively what was obtained for the two NiHf2-1 and Hf2-2 alloys the behaviors of which were very good in 3 points flexural creep at 1200°C for an induced maximal tensile stress of 20MPa. The observed creep behaviors were much better than what can be usually expected for equi-axed nickel-based alloys simply strengthened by carbides (alloys disadvantaged by regards to single-crystal Ni-based superalloys efficiently reinforced by dense gamma prime precipitation).

The behaviors in oxidation at 1100°C of the three alloys are all chromia-forming, as shown by the post-mortem characterization of the oxidized samples which showed that chromia is the predominant oxide present. It is true that the presence of other oxides was noticed (e.g. by XRD) but their fractions were obviously significantly lower than the chromia one. Essentially constituted of chromia the external scale was resistant against the growth compressive stresses which usually develop during the thickening of the scale, which inhibits all unsticking/detachment from the alloy surface. This phenomenon of unsticking from substrate is, in addition, elsewhere obstructed by the “pegging” effect of hafnium (also known with yttrium) in the case of the two Hf-containing alloys NiHf2-1 and NiHf2-2. This is the reason of the very parabolic general shape of the three mass gain curves.

Second, this predominance of chromia in term of global mass of oxide, its continuity and its direct exposure to hot air (continuous external scale) allowed applying the {$m \times dm/dt = Kp - Kv \times m$} method [47] to determine the parabolic constant Kp (without underestimation) and linear Kv constant which characterizes the volatilization rate of chromia. The obtained values of Kp and Kv values are all in the usual ranges of values typical of chromia growth and of chromia re-oxidation in volatile CrO_3, respectively. The chromia-forming behavior, one the one hand suggested by the values of Kp and Kv and on the other hand proved by the post-mortem characterization of the samples, guarantees a good resistance of the alloys against high temperature oxidation. Furthermore, the values of chromium contents in alloy close to

the extreme surface are still high, indicating that this chromia-forming behavior is not yet threatened.

However one must mention that, even if all alloys were chromia-forming, the oxidation kinetics differed from one another. In addition, by comparing to one another the mass gain curves obtained with the two HfC-reinforced alloys and second these curves with the one of the reference Hf-free alloy, it appears that there is no monotonous evolution of the oxidation kinetics versus the Hf content. Indeed the NiHf2-1 alloy, which contains 3.7 wt.%Hf, oxidized slower than the reference Hf-free NiHf2 alloy while the NiHf2-2 alloy, which contains 5.6 wt.%Hf oxidized faster than the Hf-free reference alloy. Small additions in Hf in superalloys, whatever their basis (Ni, Co Fe and other) and their elaboration procedure (casting, powder metallurgy and others) are well known as being beneficial for the high temperature oxidation behavior: around 1 wt.% Hf (even 2 wt.%) in the whole chemical composition of the alloy slows down the isothermal oxidation rate and improves the resistance against spallation; for higher amounts the presence of hafnium is less known and it is possible that these additional wt.% in Hf either promote new improvement in the oxidation behavior or, in contrast, induce a general deterioration due to a too high content in a so reactive element as Hf. Here we saw first that Hf content until almost 4 wt.% allows keeping a beneficial effect (NiHf2-1); in contrast, for more than 5 wt.% Hf we discovered in the present work that the influence has become detrimental. This can be explained as follows: the NiHf2-1 alloy benefits from the presence of Hf (usual effect) without suffering from the possible obstruction, by too many interdendritic HfC, of the Cr diffusion towards the oxidation front. Furthermore NiHfC2-1 contains significant quantity in chromium carbides which are known as being Cr reservoirs ideally located in the interdendritic spaces which are widely recognized to be efficient diffusion paths for chromium. In contrast, in the case of the NiHf2-2 alloy, almost no chromium carbides are present in the interdendritic spaces and, instead, there are supplementary HfC carbides which act as local barriers for Cr diffusion. This causes the development and maintenance of a chromia layer which is of not so good quality in terms of compactness, porosities and defects… Consequently the diffusion, through the external chromia scale, of the species involved in the oxidation phenomenon is not so limited and the oxide growth is thus faster.

Nevertheless, the oxidation rates are all rather slow for this temperature so high as 1100°C and the possible deterioration of the high temperature oxidation resistance (case of the HfC-richest alloy) does not threaten the interest of this new family of HfC-reinforced alloys which

obviously offers high creep resistance at a temperature at which even the mechanical strength of the γ/γ' single crystal alloys can be rather low.

5. Conclusions

Thus, choosing Hf, not for its beneficial effect on the high temperature oxidation behavior of alloys, but for obtaining an interdendritic network of script MC-carbides mixed with the periphery of the matrix dendrites, allows not only obtaining oxidation-resistant Cr-rich nickel-based alloys, but also presenting remarkable creep resistance. This was here demonstrated for service at 1100°C, temperature at which the γ' precipitates of Ni-based single crystals can be totally dissolved. Thus, although still simple (only four elements in their composition), these alloys are maybe able to be employed in concurrence with these Ni-based single-crystals at 1100°C in some cases. Furthermore, their high content in chromium should give them good resistance against corrosion by molten substances as molten glasses. Additional developments are probably required to optimize them for such goals, by defining more sophisticated chemical compositions (e.g. solid solution strengthening) and by applying precipitation heat-treatments (e.g. hardening by secondary carbides). Concerning the creep phenomena this work opens possibilities for future deeper investigations for interpreting the differences in creep behavior, and finding the reasons of the particularly interesting properties of these HfC-strengthened alloys. Among the suggested outlooks one can think carrying out thorough examinations of the deformed zones of the samples in order to understand the differences in mechanisms of deformation and, if any, the ones governing the crack initiation and propagation (fractography high magnification SEM/Secondary Electrons observations, Transmission Electron Microscopy observations of dislocations and characterization of the characteristics of the final Franck network…). Special attention can be brought to the importance of keeping the script-like shape of the MC carbides on long times at high temperature, to totally explain the superiority of HfC on other MC carbides such as TaC.

Acknowledgments

The authors wish to thank Pascal Villeger who carried out the X-ray diffraction runs.

REFERENCES

[1] M.J. Donachie, S.J. Donachie, Superalloys: A Technical Guide (2nd edn.), ASM International, Materials Park (2002).

[2] A.A. Hopgood, A. Nicholls, G.D.W. Smith, J.W. Martin, Effects of heat treatment on phase chemistry and microstructure of single crystal nickel base superalloy, Mater. Sci Technol 46 (1988) 146-52.

[3] S. Polsilapa, P. Sopon, N. Panich, N. Chuankrerkkul, A. Thueploy, Reheat treated microstructures and gamma prime particle coarsening behaviour at 900°C of cast nickel based superalloy IN-738, JOM 16 (2006) 7-13.

[4] M. Doi, T. Kozakai, T. Moritani, S. Naito, Two-phase microstructures of gamma+gamma-prime formed by phase-separations due to heat-treatments of elastically constrained Ni-Al-Ti alloys, Mater. Sci. Forum 539-543 (2006) 3006-3011.

[5] A. Devaux, L. Naze, R. Molins, A. Pineau, A. Organista, J.-Y. Guedou, J.F. Uginet, P. Heritier, Gamma double prime precipitation kinetic in Alloy 718 Mater. Sci. Eng. A, A486 (2008) 117-122.

[6] P. Wangyao, S. Polsilapa, P. Chaishom, J. Zrnik, W. Homkrajai, N. Panich, Gamma prime particle coarsening behavior at elevated temperatures in cast nickel-based superalloy GTD-111 EA, High Temp. Mater. Processes 27 (2008) 41-49.

[7] E.J. Payton, T.A. Wynn, M.J. Mills, Experimental measurement of the kinetics of gamma prime dissolution during supersolvus heat treatment of powder metallurgical Ni-based disk superalloys, J. Mater. Sci. 47 (2012) 7305-7311.

[8] B. Wang, F. Zhang, W. Cao, S. Chen, S. Kou, Computational kinetics simulation of precipitation and dissolution of gamma prime (γ') in heat treating and welding of 718plus superalloy, Metall. Mater. Trans. A 46 (2015) 115-122.

[9] D. Young D, High Temperature Oxidation and Corrosion of Metals, Elsevier Corrosion Series, Amsterdam (2008).

[10] D. Bozic, M. Mitkov, N. Ilic, Z. Bogdanov, M.T. Jovanovic, Microstructure and mechanical properties of nickel aluminide (Ni_3Al) base intermetallic compound produced by PM and standard casting procedure, Science of Sintering 24 (1992) 191-197.

[11] P. Perez, J.L. Gonzalez-Carrasco, P. Adeva, Influence of exposure time and grain size on the oxidation behavior of a PM Ni_3Al alloy at 635°C, Corros. Sci. 40 (1998) 631-644.

[12] H.G. Kim, S.S. Kim, I.S. Ahn, M.W. Park, The effect of grain size on the elevated temperature tensile behavior of MA/PM Al-8.5Fe-1.3V-1.7Si alloys, J. Mater. Sci. Lett. 19 (2000) 65-68.

[13] J.M. Silva, R.A. Claudio, A. Sousa e Brito, C.M. Branco, J. Byrne, Characterization of powder metallurgy (PM) nickel base superalloys for aeronautical application, Mater. Sci. Forum 514-516 (2006) 495-499.

[14] Z.Q. Cao, Y. Sun, H.J. Sun, Effect of grain size on oxidation behavior of Fe-40Ni-15Cr alloys, High Temp. Mater. Processes 31 (2012) 83-87.

[15] J. Li, Y. Liu, B. Liu, Y. Wang, X. Liang, Y. He, Microstructure characterization and mechanical behaviors of a hot forged high Nb containing PM-TiAl alloy, Mater. Charact. 95 (2014) 148-156.

[16] C.P. Cutler, S.W.K. Shaw, The interrelationship γ' size, grain size and mechanical properties in IN-939 a cast nickel-base superalloy, Strength Met. Alloys, Proc. Int. Conf., 5th, (Edited by Haasen, Peter; Gerold, V.; Kostorz, G) 2 (1979) 1357-1362.

[17] F. Meyer-Olbersleben, F. Rezai-Aria, B. Ilschner, The effect of grain size and upper cycle temperature on the thermal fatigue behavior of IN 100 superalloy, High Temp. Mater. Power Eng. 1990, Proc. Conf. (Edited by Bachelet, E) 2 (1990) 1121-1129.

[18] A. Baldan, Effects of grain size and carbides on the creep resistance and rupture properties of a conventionally cast nickel-base superalloy, Z. Metallkd. 83 (1992) 750-757.

[19] A. Baldan, Combined effects of thin-section size, grain size and cavities on the high temperature creep fracture properties of a nickel-base superalloy J. Mater. Sci. 32 (1997) 35-45.

[20] Z. Pei, M. Zhao, Y. Tian, J. Li, X. Chen, J. Wu, Effect of melt superheating treatment on the cast structure of K465 nickel-based superalloy, Rare Metals 28 (2009) 193-196.

[21] B. Du, J. Yang, C. Cui, X. Sun X, Effects of grain size on the high-cycle fatigue behavior of IN792 superalloy, Mater. Des. 65 (2015) 57-64.

[22] C. Tian, G. Han, C. Cui, X. Sun, Effects of Co content on tensile properties and deformation behaviors of Ni-based disk superalloys at different temperatures, Mater. Des. 88 (2015) 123-131.

[23] H. Zhang, K. Zhang, H. Zhou, Z. Lu, C. Zhao, X. Yang, Effect of strain rate on microstructure evolution of a nickel-based superalloy during hot deformation, Mater. Des. 80 (2015) 51-62.

[24] X.-M. Chen, Y.C. Lin, M.-S. Chen, H.-B. Li, D.-X. Wen, J.-L. Zhang, M. He, Microstructural evolution of a nickel-based superalloy during hot deformation, 77 (2015) 41-49.

[25] T.A. Myles, F. Knee, New high chrome fused cast refractory for use in contact with highly corrosive glasses, Ceramic Engineering and Science Proceedings 7 (1986) 269-276.

[26] T.M. Wehrenberg, C.N. McGarry, New AZS chromic oxide refractory for wool fiber-glass melting furnaces, Ceramic Engineering and Science Proceedings 9 (1988) 82-90.

[27] B. Tian, C. Lind, O. Paris, Influence of $Cr_{23}C_6$ carbides on dynamic recrystallization in hot deformed Nimonic 80a alloys, Mater. Sci. Eng. A, A358 (2003) 44-51.

[28] H.Y. Bor, C.N. Wei, R.R. Jeng, P.Y. Ko, Elucidating the effects of solution and double ageing treatment on the mechanical properties and toughness of MAR-M247 superalloy at high temperature Mater. Chem. Phys. 109 (2008) 334-341.

[29] H.R. Zhang, O.A. Ojo, Cr-rich nanosize precipitates in a standard heat-treated Inconel 738 superalloy Philos. Mag. 90 (2010) 765-782.

[30] A. Strondl, S. Milenkovic, A. Schneider; U. Klement, G. Frommeyer G, Effect of Processing on Microstructure and Physical Properties of Three Nickel-Based Superalloys with Different Hardening Mechanisms, Adv. Eng. Mater. 14 (2012) 427-438.

[31] H. Bibring, J.P. Trottier, M. Rabinovitch, G. Seibel, Unidirectional solidification of cobalt-chromium and nickel-chromium alloys reinforced by non-crystalline tantalum carbide. Structures and properties, Rev. Met. / Mem. Sci. 68 (1971) 23-41.

[32] J.L. Walter, E. Cline Harvey, Structures and properties of cobalt-base tantalum carbide eutectic alloys, Metall. Trans. 4 (1973) 1775-1784.

[33] P. Berthod, S. Michon, L. Aranda, S. Mathieu, J.C. Gachon, Experimental and thermodynamic study of the microstructure evolution in cobalt-base superalloys at high temperature Calphad 27 (2003) 353-359.

[34] M. Montazeri, M. Ghaini Farshid, A. Farnia, An investigation into the microstructure and weldability of a tantalum-containing cast cobalt-based superalloy, Int. J. Mater. Res. 102 (2011) 1446-1451.

[35] P. Berthod, L. Aranda, C. Vebert, S. Michon, Experimental and thermodynamic study of the high temperature microstructure of tantalum containing nickel-based alloys Calphad 28 (2004)159-166.

[36] W. Sun, X. Qin, J. Guo, L. Lou, L. Zhou, Thermal stability of primary MC carbide and its influence on the performance of cast Ni-base superalloys, Mater. Des. 69 (2015) 81-88.

[37] M. R. Jahangiri, M. Abedini, Effect of long time service exposure on microstructure and mechanical properties of gas turbine vanes made of IN939 alloy, Mater. Des. 64 (2014) 588-600.

[38] C. Yang, Y. Xu, H. Nie, X. Xiao, G. Jia, Z. Shen, Effects of heat treatments on the microstructure and mechanical properties of Rene 80, Mater. Des. 43 (2013) 66-73.

[39] C. Ribaudo, J. Mazumder, Oxidation behavior of a laser-clad nickel-based alloy containing hafnium Mater. Sci. Eng. A120-121 (1989) 531-538.

[40] H.L. Du, J. Kipkemoi, D.N. Tsipas, P.K. Datta, The high temperature corrosion behavior of Hf modified chromo-aluminized coatings produced by a single step process Surf. Coat. Technology 86-87 (1996) 1-8.

[41] J.Y. Zhong, R.D. Mu, L.M. He, High temperature oxidation behaviour of plasma carburised Ni based single crystal superalloy with NiCoCrAlYHf high temperature oxidation protective coatings, Mater. Res. Innovations 18 (2014) S4-1115-S4-1120.

[42] H.E. Zschau, F. King, M.C. Galetz, M. Schütze, Implantation of Y- and Hf-ions into a F-doped Ni-base superalloy improving the oxidation resistance at high temperatures, Nucl. Instrum. Methods Phys. Res., Sect. B doi:10.1016/j.nimb.2015.07.080

[43] P. Berthod, Hafnium carbides in cast chromium-rich refractory alloys. Part 1: case of nickel-based alloys, Mater. Sci.: An Ind. J. 9 (2013) 359-365.

[44] P. Berthod, E. Conrath, Microstructure evolution in bulk and surface states of chromium rich nickel based cast alloys reinforced by hafnium carbides after exposure to high temperature air, Mater. High Temp. 31 (2014) 266-273.
[45] E. Conrath, P. Berthod, Kinetics of high temperature oxidation and chromia volatilization for HfC-containing nickel-based alloys, Oxid. Met. 81 (2014) 393-405.
[46] P. Berthod, E. Conrath, Mechanical and chemical properties at high temperature of {M-25Cr}-based alloys containing hafnium carbides (M=Co, Ni or Fe): creep behavior and oxidation at 1200°C J. Mater. Sci. Technol. Res. 1 (2014) 7-14, doi:10.15377/2410-4701.2014.01.01.2
[47] P. Berthod, Kinetics of high temperature oxidation and chromia volatilization for a binary Ni-Cr alloy, Oxid. Met. 64(3-4) (2005) 235-252.

List of the Tables

Table 1. Names and chemical compositions of the three alloys studied in this work
(all contents in weight.%)

elements	Cr	C(expected)	Hf
NiHf2	25	0.5	/
NiHf2-1	25	0.5	3.7
NiHf2-2	25	0.5	5.6

Table 2. Surface fractions of carbides in the three as-cast alloys studied in this work
(average and standard deviation values from three ×1000 SEM/BSE micrographs)

Surf.%	Hafnium carbides	Chromium carbides
NiHf2	/	5.0 ±1.2
NiHf2-1	4.7 ±0.6	2.6 ±0.3
NiHf2-2	6.9 ±0.2	0.3 ±0.1

Table 3. Values of the constants describing the oxidation kinetics of the three studied alloys at 1100°C

Constants	K_l ($\times 10^{-8}$ g cm^{-2} s^{-1})	K_p ($\times 10^{-12}$ g^2 cm^{-4} s^{-1})		K_l ($\times 10^{-10}$ g cm^{-2} s^{-1})
Alloys	slope at stage start	classic	m × dm/dt = f(-m)	m × dm/dt = f(-m)
NiHf2	19.8	5.50	10.5	46.3
NiHf2-1	10.4	1.32	7.84	101
NiHf2-2	20.6	10.6	34.8	150

Table 4. Values of contents in Cr and Hf in alloy at the oxide/substrate interface for the three studied alloys

Elements in extreme surface	Average wt.%Cr	Std deviation wt.%Cr	wt.%Hf range
NiHf2	18.1	1.0	/
NiHf2-1	23.1	0.2	0-0.82
NiHf2-2	22.3	0.2	0-1.47

List of the Figures

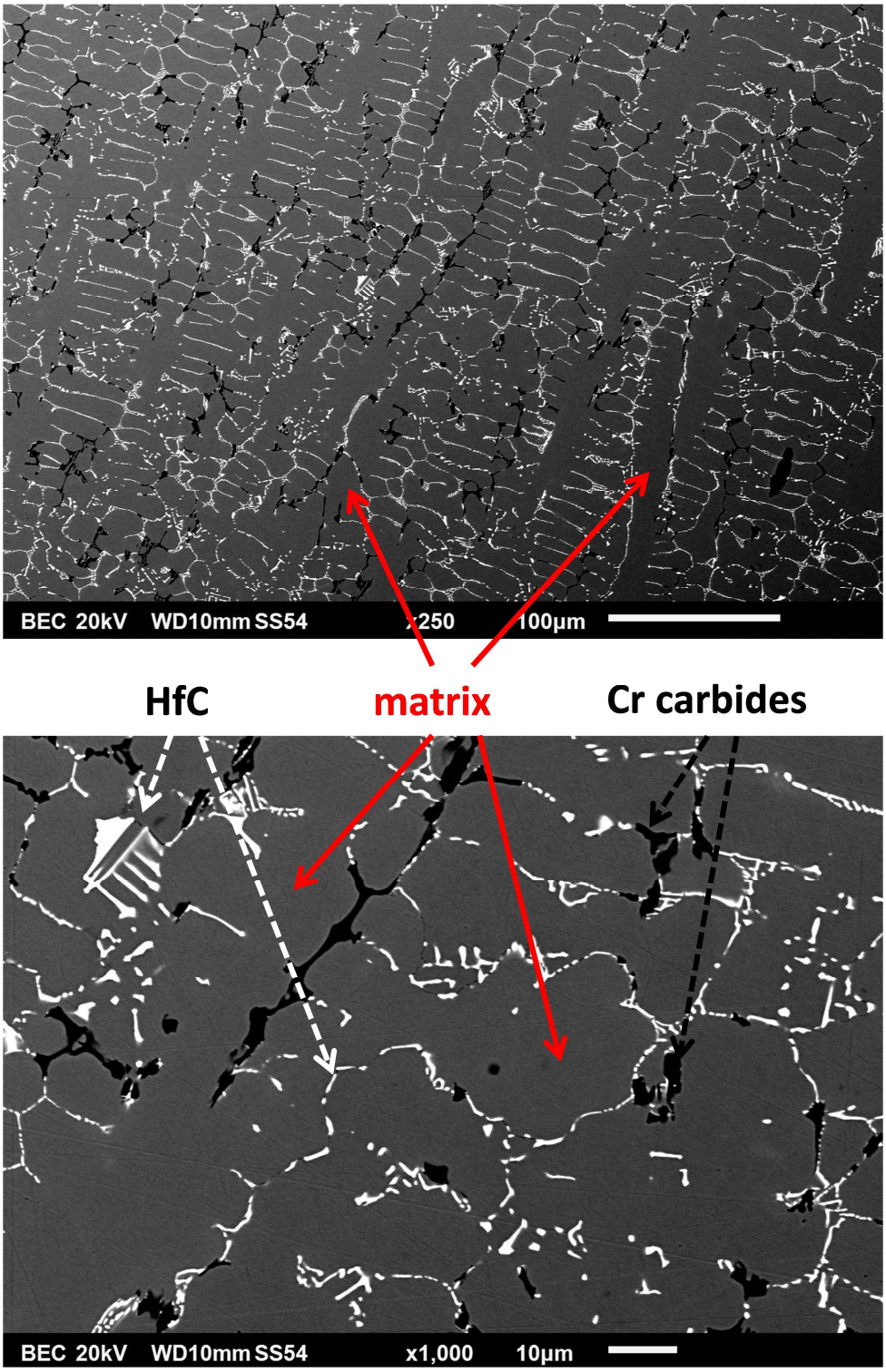

Fig. 1. As-cast microstructure of the NiHf2-1 alloy (SEM/BSE micrographs)

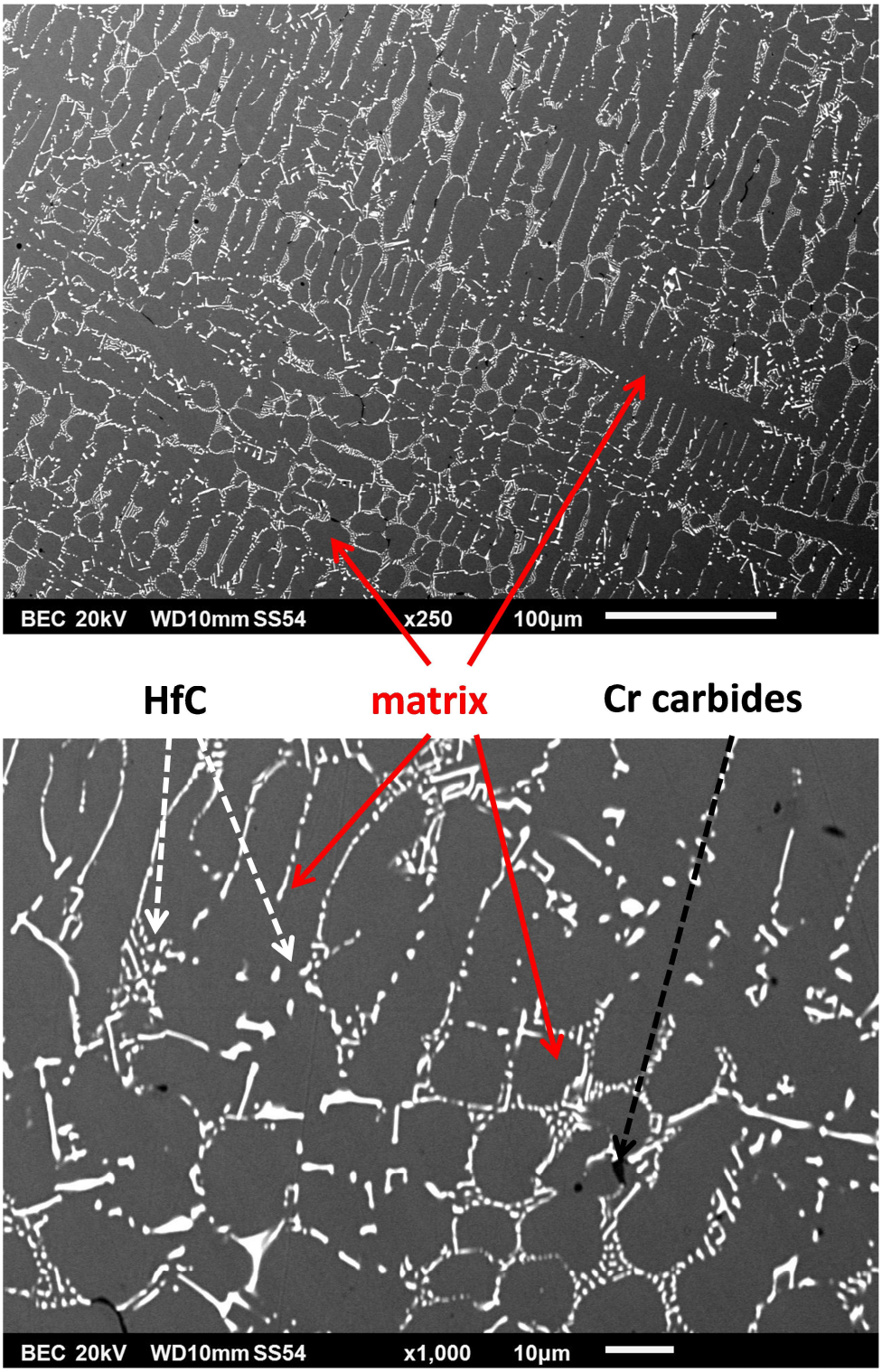

Fig. 2. As-cast microstructure of the NiHf2-2 alloy (SEM/BSE micrographs)

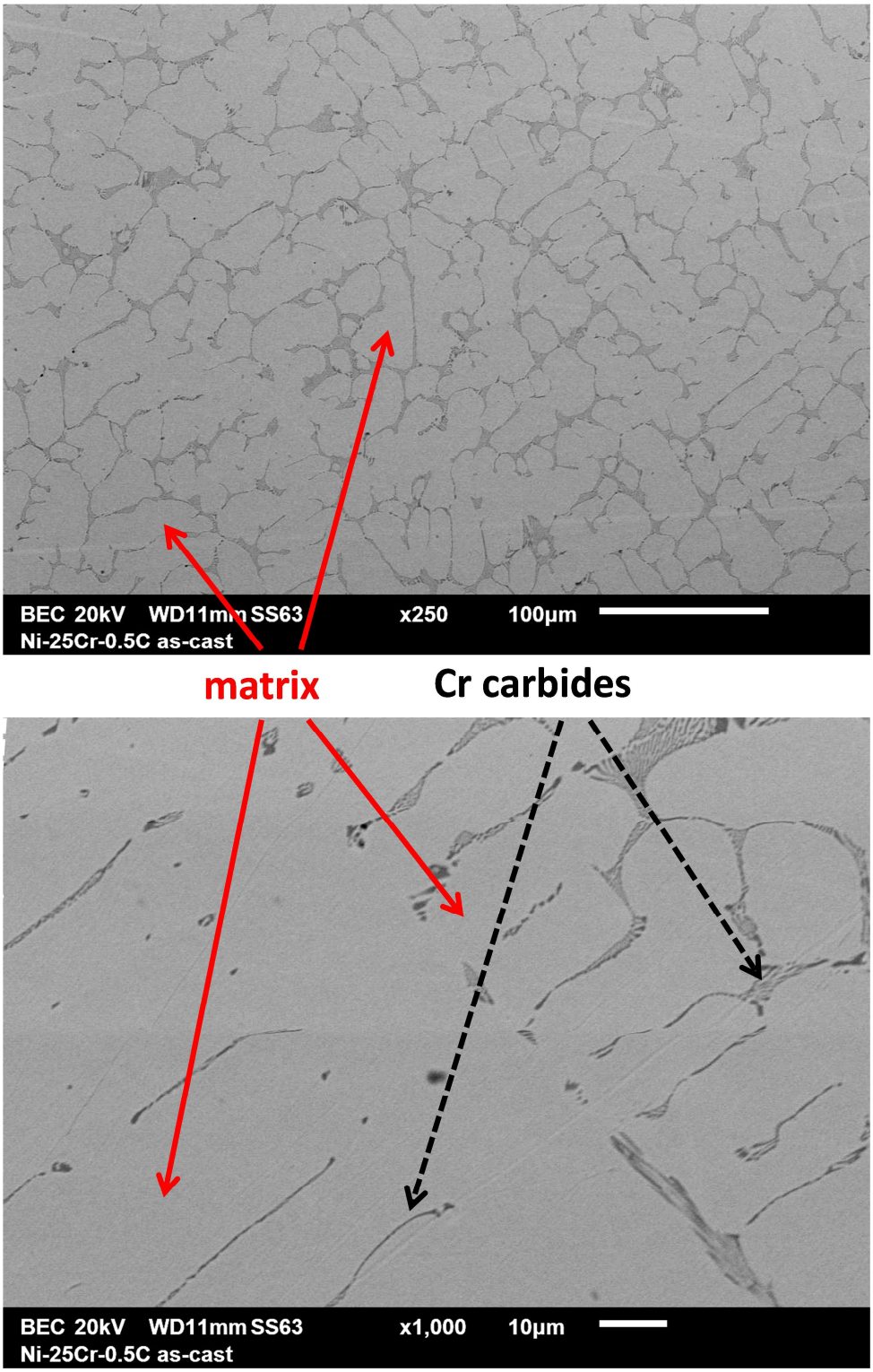

Fig. 3. As-cast microstructure of the reference NiHf2 alloy (SEM/BSE micrographs)

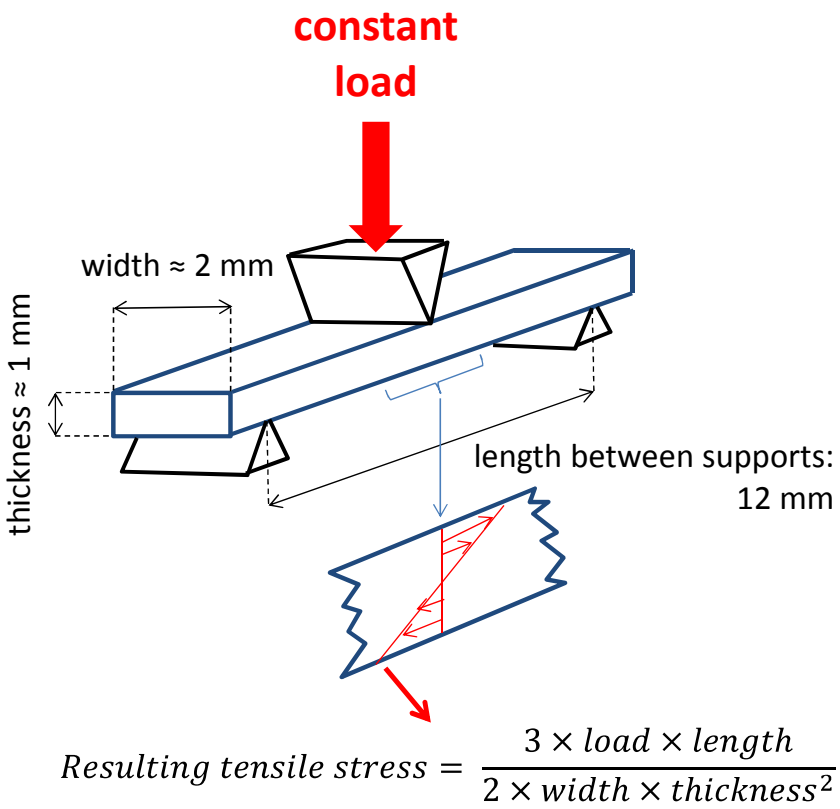

Fig. 4. Scheme reminding the principle of 3-points flexural tests, average dimensions of the parallelepiped samples and formula allowing the load determination to obtain the targeted value of the local maximal tensile stress

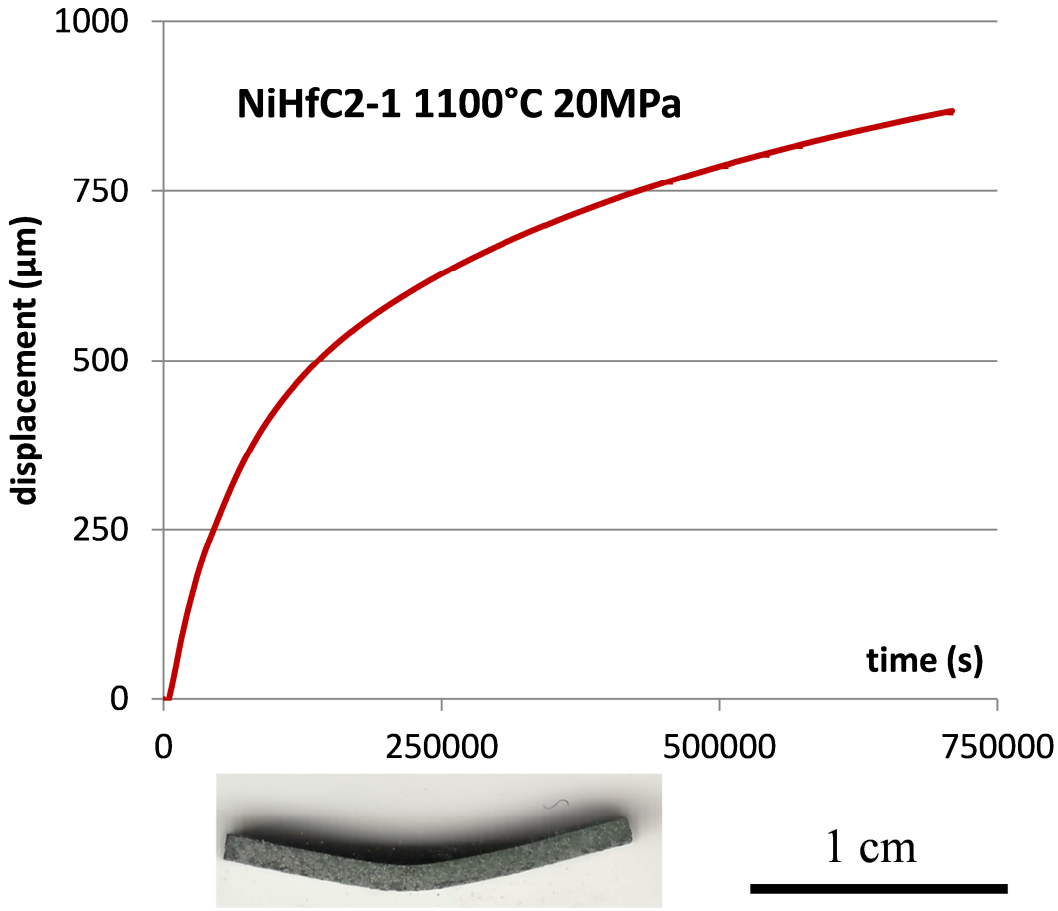

Fig. 5. Three-points flexural creep deformation curve obtained for the NiHfC2-1 alloy at 1100°C for 20MPa of resulting tensile stress; general view of the deformed sample

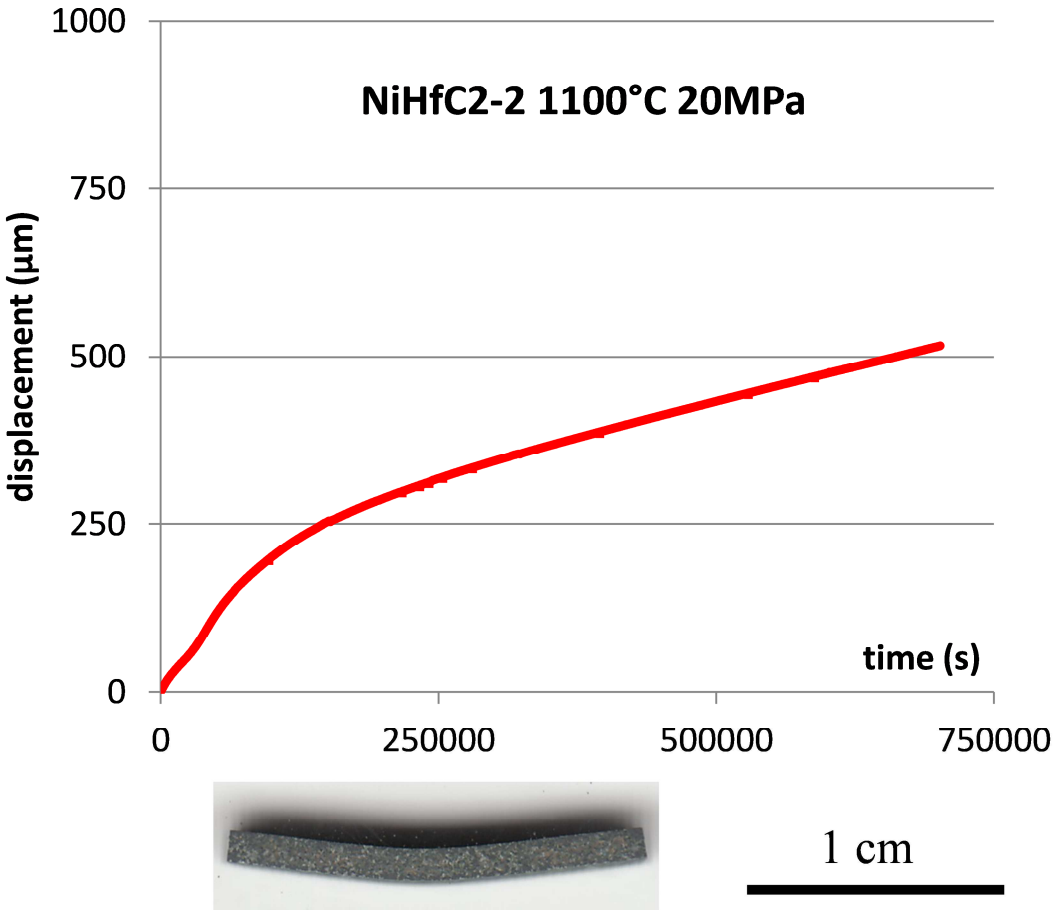

Fig. 6. Three-points flexural creep deformation curve obtained for the NiHfC2-2 alloy at 1100°C for 20MPa of resulting tensile stress; general view of the deformed sample

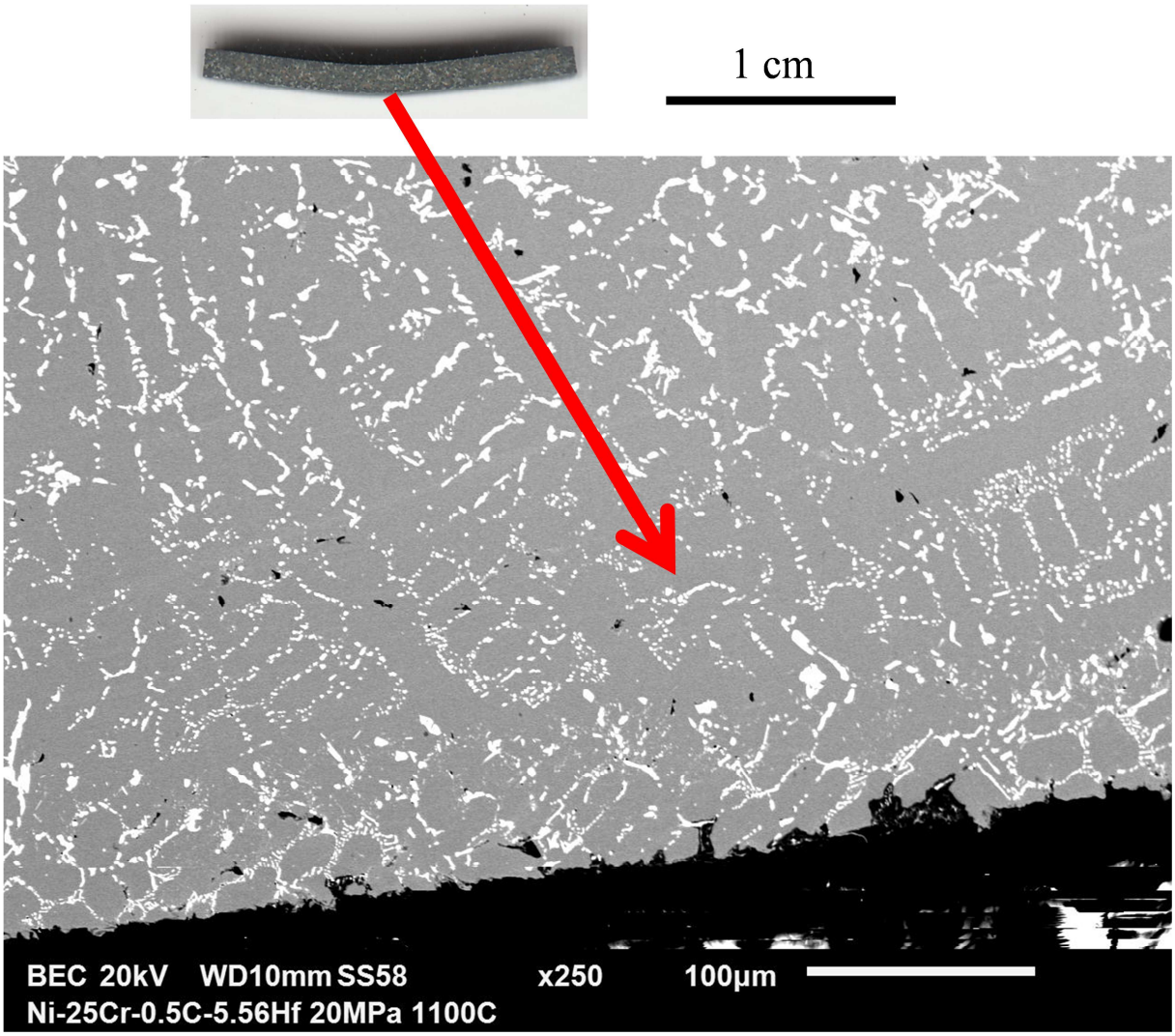

Fig. 7. General view of the deformed NiHf2-1 and NiHf2-2 samples; local microstructure of the deformed NiHf2-2 and surface state of the part of this sample which was the most solicited by tensile stress (20MPa) (middle bottom side of the deformed parallelepiped)

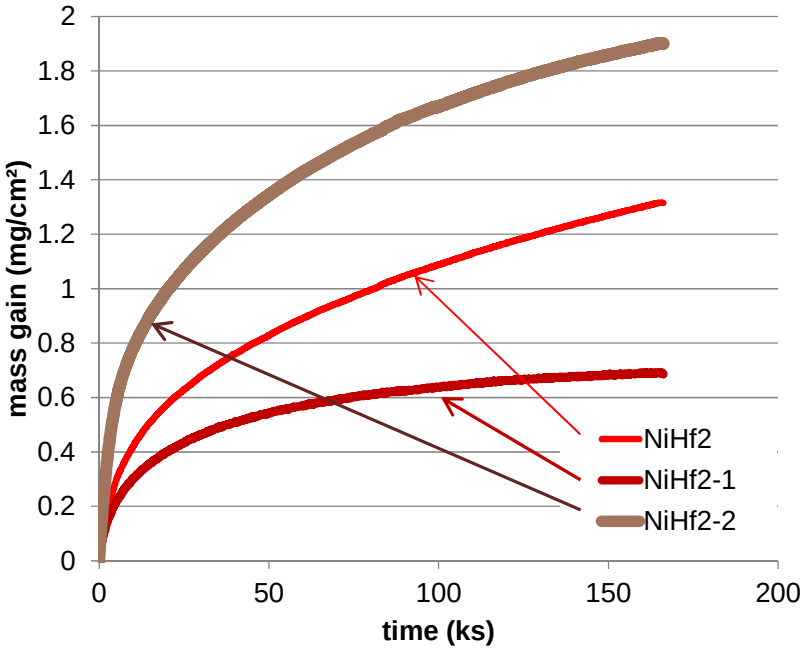

Fig. 8. Mass gain curves obtained during the thermogravimetric oxidation tests of the three alloys at 1100°C dry in air

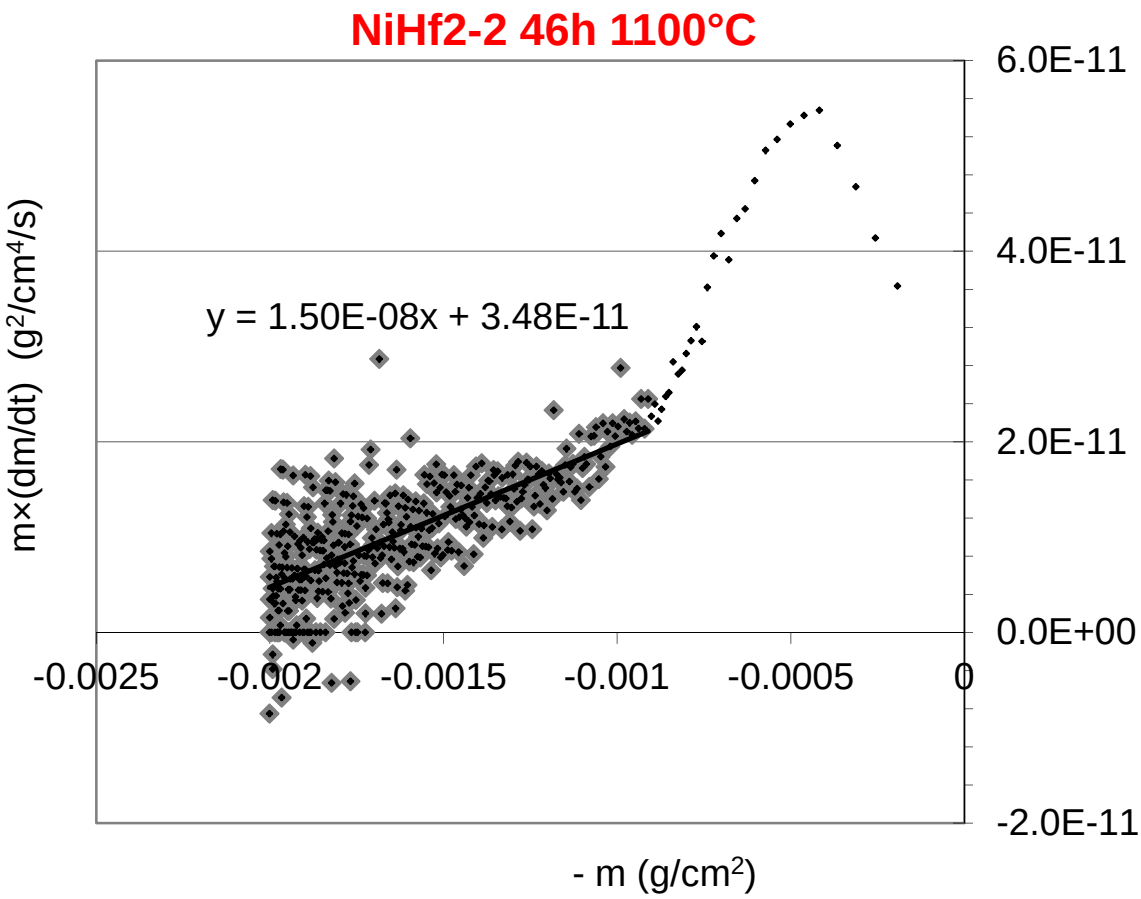

Fig. 9. Example of determination of the k_p and k_v oxidation constants according to the {m×dm/dt = K_p - K_v × m} method;

here, for the NiHf2-2 alloy: $K_p = 34.8 \times 10^{-12}$ g^2 cm^{-4} s^{-1} and $K_v = 150 \times 10^{-10}$ g cm^{-2} s^{-1}

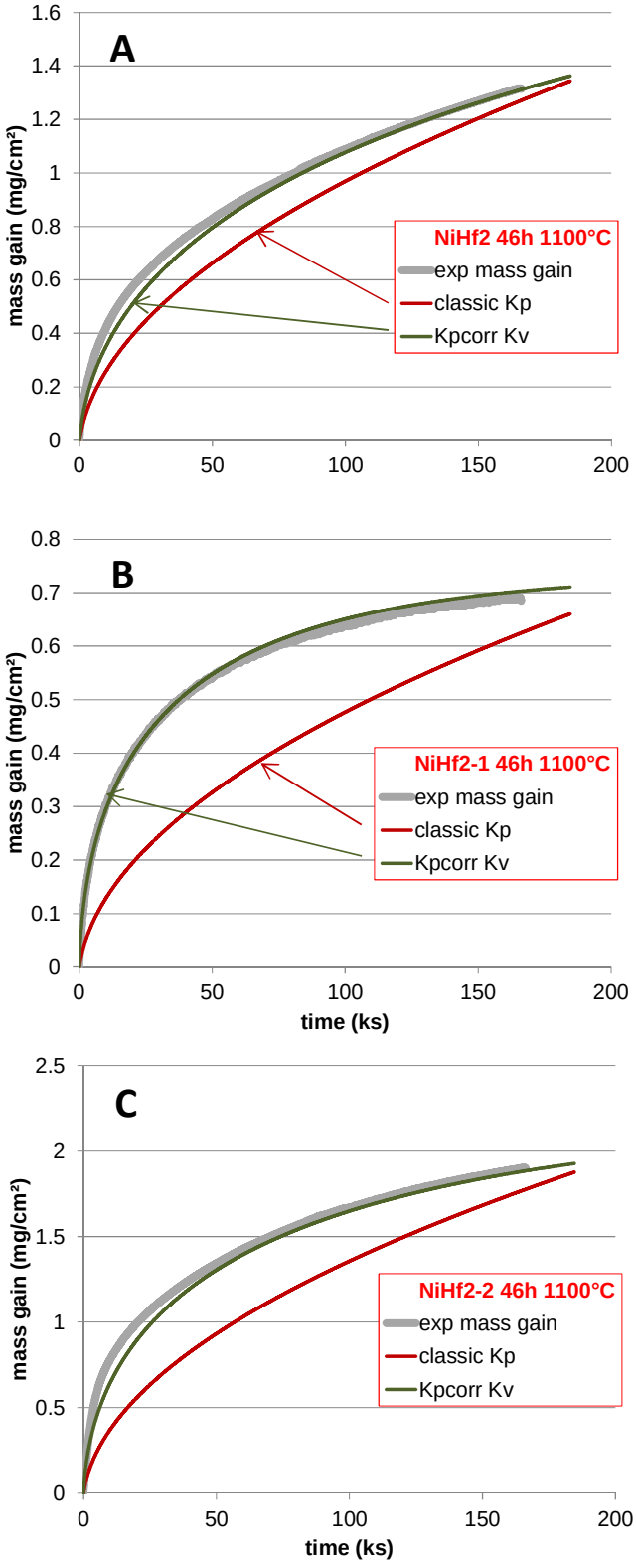

Fig. 10. Comparison between the mathematical curves plotted from the determined values of the K_p constant, classically determined or determined according to the {m×dm/dt = K_p - K_v × m} method, and the K_v constant, and the experimental mass gain curve, for the three alloys NiHf2 (A), NiHf2-1 (B) and NiHf2-2 (C)

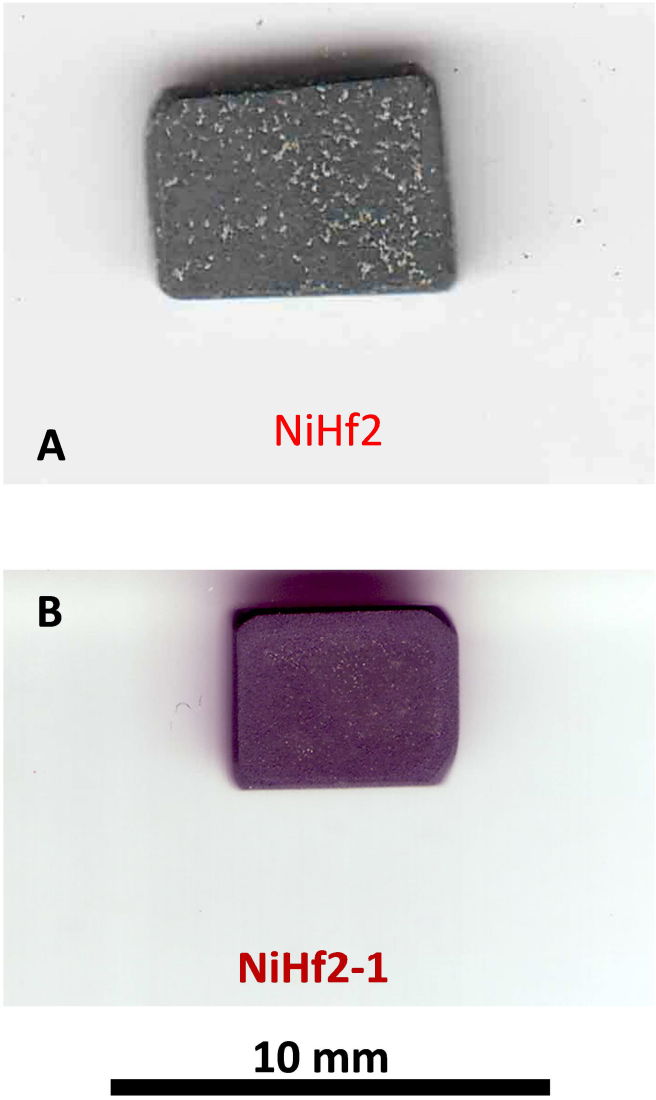

Fig. 11. Comparison of surface states between the oxidized Hf-free alloy (NiHf2 (A): oxide spallation) and of one of the two oxidized Hf-containing alloys (NiHf2-1 (B): no spallation)

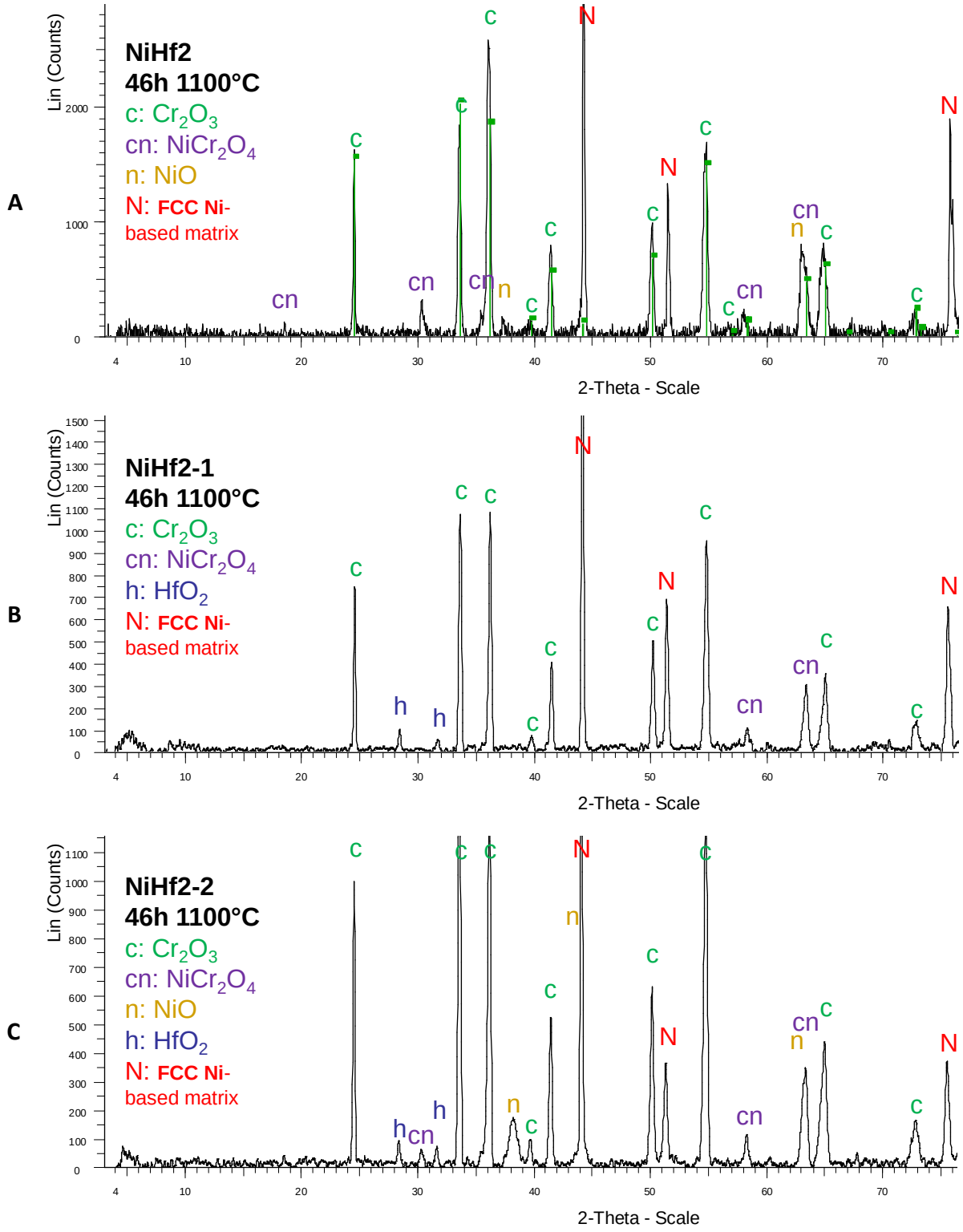

Fig. 12. X-ray diffractograms obtained on the oxidized surfaces of the three alloys, NiHf2 (A), NiHf2-1 (B) and NiHf2-2 (C)

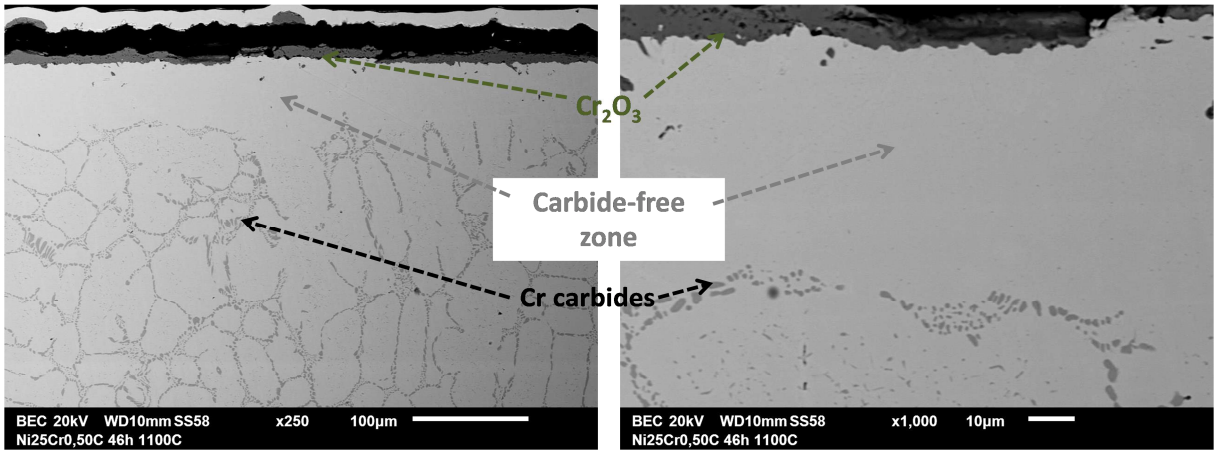

NiHf2

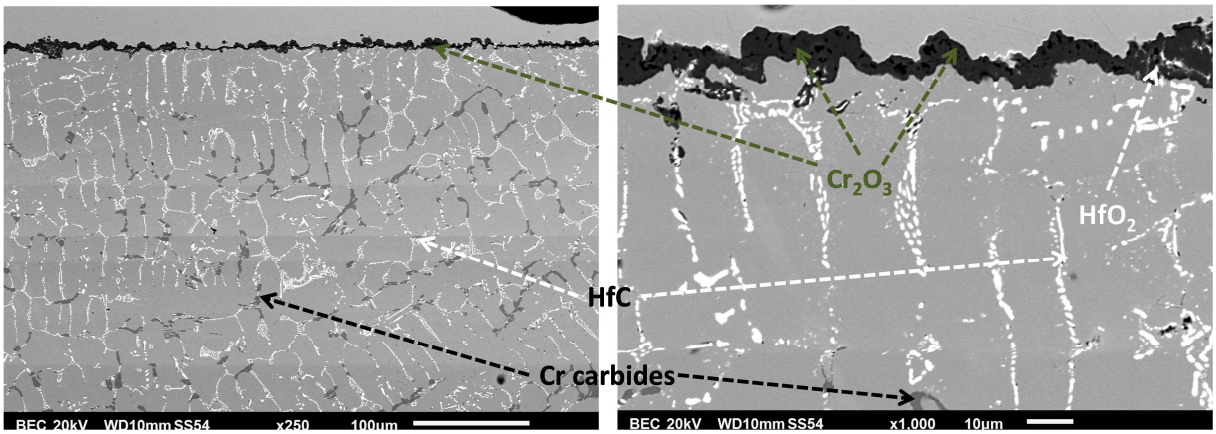

NiHf2-1

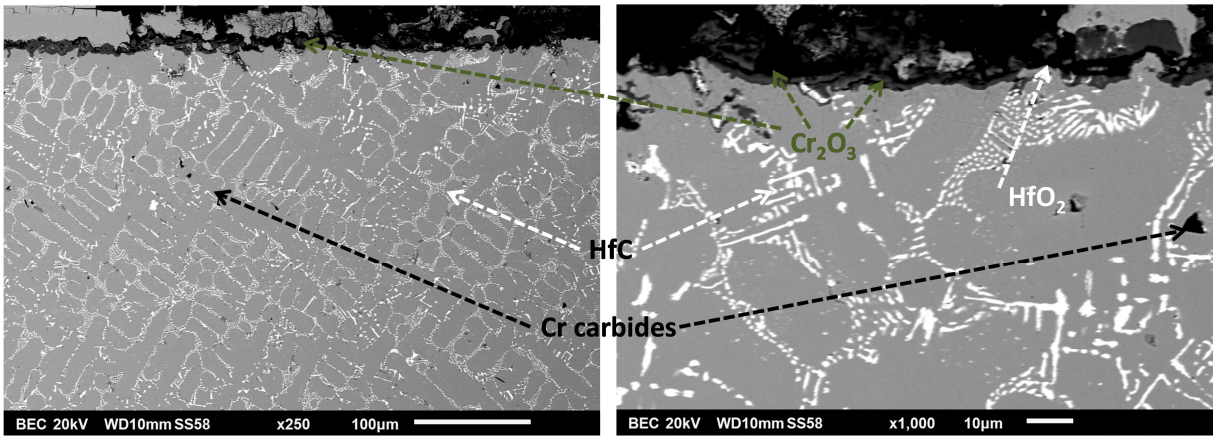

NiHf2-2

Fig. 13. Cross-sectional view of the oxidized surface and subsurface of the NiHf2 (top), NiHf2-1 (middle) and NiHf2-2 (bottom) alloys (SEM/BSE micrographs)